Atmos. Chem. Phys. Discuss., 11, 10087–10120, 2011
www.atmos-chem-phys-discuss.net/11/10087/2011/
doi:10.5194/acpd-11-10087-2011

Atmospheric Chemistry and Physics Discussions

Temporal and spatial variability of the stable isotopic composition of atmospheric molecular hydrogen: observations at six EUROHYDROS stations

A. M. Batenburg[1], S. Walter[1], G. Pieterse[1], I. Levin[2], M. Schmidt[3], A. Jordan[4], S. Hammer[2], C. Yver[3], and T. Röckmann[1]

[1]Institute for Marine and Atmospheric Research Utrecht, Utrecht University, Utrecht, The Netherlands
[2]Institut für Umweltphysik, University of Heidelberg, Heidelberg, Germany
[3]Laboratoire des Sciences du Climat et de l'Environnement, Gif sur Yvette, France
[4]Max Planck Institut für Biogeochemie, Jena, Germany

Received: 7 March 2011 – Accepted: 18 March 2011 – Published: 29 March 2011

Correspondence to: A. M. Batenburg (a.m.batenburg@uu.nl)

Published by Copernicus Publications on behalf of the European Geosciences Union.

Abstract

Despite the potential of isotope measurements to improve our understanding of the global atmospheric molecular hydrogen (H_2) cycle, few H_2 isotope data have been published so far. Now, within the EUROpean network for atmospheric HYDRogen Observations and Studies project (EUROHYDROS), weekly to monthly air samples from six locations in a global sampling network have been analysed for hydrogen mixing ratio ($m(H_2)$) and the stable hydrogen isotopic composition of H_2 ($\delta(D,H_2)$, hereafter referred to as $\delta(D)$). The time series thus obtained now cover one to five years for all stations. This is the largest set of ground station observations of $\delta(D)$ so far. Annual average $\delta(D)$ values are higher at the Southern Hemisphere (SH) than at the Northern Hemisphere (NH) stations; the maximum is observed at Neumayer (Antarctica), and the minimum at the NH midlatitude or subtropical stations. The maximum seasonal differences in $\delta(D)$ range from ≈18‰ at Neumayer to ≈45‰ at Schauinsland (Southern Germany); in general, seasonal variability is largest at the NH stations. The timing of minima and maxima differs per station as well. In Alert (Arctic Canada), the variations in $\delta(D)$ and $m(H_2)$ can be approximated as simple harmonic functions with a ≈5-month phase shift. This out-of-phase seasonal behaviour of $\delta(D)$ and $m(H_2)$ can also be detected, but with a ≈6-month phase shift, at Mace Head and Cape Verde. However, no seasonal $\delta(D)$ cycle could be observed at Schauinsland, which likely reflects the larger influence of local sources and sinks at this continental station. At the two SH stations, no seasonal cycle could be detected in the $\delta(D)$ data. Assuming that the sink processes are the main drivers of the observed seasonality in $m(H_2)$ and $\delta(D)$ on the NH, the relative seasonal variations can be used to estimate the relative sink strength of the two major sinks, deposition to soils and atmospheric oxidation by the hydroxyl (OH) radical. For the NH coastal and marine stations this analysis shows that the relative contribution of soil uptake to the total sink processes increases with latitude.

ACPD

11, 10087–10120, 2011

1 Introduction

Molecular hydrogen (H_2) is present in the atmosphere with a mixing ratio of ≈0.5 ppm (μmole mole^{-1}) (Glueckauf and Kitt, 1957; Schmidt and Seiler, 1970; Schmidt, 1974; Ehhalt et al., 1977). Over the last decades, several studies examined the magnitude of the source and sink terms in the global H_2 budget (Table 1) (Novelli et al., 1999; Rhee et al., 2006b; Price et al., 2007; Ehhalt and Rohrer, 2009; Pieterse et al., 2011). These show that the largest H_2 sources are the atmospheric oxidation of methane and other hydrocarbons, and combustion processes. Production by nitrogen-fixing bacteria, on land or in the oceans, constitutes a smaller source. About three quarters of the H_2 thus produced is taken up by soil; the other quarter is oxidized by the hydroxyl radical (OH). However, large quantitative uncertainties still exist in the global H_2 budget. For example, the estimates for the sink strength of soil uptake – the largest term in the budget – vary widely between these estimates.

Research into the atmospheric H_2 budget has increased in recent years, because H_2 may become an important energy carrier in the future. In this case, emissions of H_2 to the atmosphere are likely to rise as a result of the inevitable leakage during production, storage and distribution of H_2 (Schultz et al., 2003). The associated rise of atmospheric H_2 levels is expected to affect the oxidative capacity of the atmosphere, with implications for the atmospheric lifetime of many species, including the strong greenhouse gas methane. Higher concentrations of H_2 will also affect stratospheric ozone levels, although estimates of the impact vary significantly among authors (Tromp et al., 2003; Warwick et al., 2004; Feck et al., 2008).

Due to the large relative mass difference between deuterated hydrogen (HD) and non-deuterated hydrogen (HH), particularly large isotope effects occur in the chemical processes that produce or remove H_2. These result in very different isotopic signatures for H_2 produced by combustion processes, by oxidation sources or by biological processes (see Table 1). For this reason, determination of the isotopic composition is a promising addition to H_2 mixing ratio observations to distinguish between different H_2

ACPD
11, 10087–10120, 2011

source and sink processes and to constrain the terms in the global budget (Gerst and Quay, 2000, 2001; Rahn et al., 2003). In this paper, the following definition of δ(D) is used to indicate the isotopic composition of the hydrogen:

$$\delta(\mathrm{D}) = \delta(\mathrm{D},\mathrm{H_2}) = \left(\frac{R_{\mathrm{Sample}}}{R_{\mathrm{VSMOW}}} - 1\right) \cdot 1000‰ \quad (1)$$

Where R_{Sample} is the ratio of the number density of deuterium atoms to the number density of "light" hydrogen atoms (H) in the H_2 of the sample, and R_{VSMOW} is the ratio of the number density of deuterium atoms to the number density of H atoms in Vienna Standard Mean Ocean Water (which is (155.76 ± 0.1) ppm). Note that the ‰-sign is explicitly included in this formula.

Following up the initial work by (Ehhalt, 1966; Gerst and Quay, 2000, 2001), new analytical techniques that have become available recently have significantly simplified isotope analysis so that many more data have become available in the past few years (Rahn et al., 2002b; Rhee et al., 2004). They have led to new constraints on the isotopic composition of H_2 from the most important sources and sinks. The isotopic composition of H_2 from CH_4 oxidation was first examined by measurements in the stratosphere (Rahn et al., 2003; Röckmann et al., 2003; Rhee et al., 2006a), but also individual steps in the oxidation sequence have been investigated, especially photolysis of formaldehyde (HCHO) (Feilberg et al., 2007; Nilsson et al., 2007; Rhee et al., 2008; Röckmann et al., 2010b). Furthermore, more information on the main surface sources, biomass burning and fossil fuel combustion (Röckmann et al., 2010a; Vollmer et al., 2010) and the largest sink, uptake in soil (Rahn et al., 2002a), has become available.

At the same time, H_2 and δ(D) have been incorporated into chemical transport models (Price et al., 2007; Pieterse et al., 2009, 2011). Until now, δ(D) measurements to validate these model results have been scarce. Data have been published from Pacific Ocean transects, the Cheeka Peak observatory (Washington, US) and the Point Barrow observatory (Alaska, US) and the CARIBIC aircraft sampling program (Gerst and Quay, 2000; Rhee et al., 2006b; Rice et al., 2010). These datasets have limited spatial

ACPD
11, 10087–10120, 2011

coverage and temporal resolution, most notably in the higher latitudes of the NH. Here we present observations from six ground stations covering high latitudes of both the NH and SH and all seasons, that will contribute to the closing of this observational gap. The interpretation of the isotope record we present here is semi-quantitative. A more rigorous quantification of the terms in the global budget will require the use of the aforementioned global chemistry models. Our data have already been used with the global chemistry transport model TM5 (Pieterse et al., 2011).

2 Experimental

Air samples were collected by the Institut für Umweltphysik of the University of Heidelberg (UHEI-IUP), the Max Planck Institute for Biogeochemistry in Jena (MPI-BGC) and the Laboratoire des Sciences du Climat et de l'Environnement in Gif-sur-Yvette (LSCE) at the six stations listed in Table 2 and depicted in Fig. 1. These six stations are part of the EUROpean network for atmospheric HYDRogen Observations and Studies (EUROHYDROS) (Engel, 2009). 1 litre or 2 litre glass flasks with Kel-F (PCTFE) o-ring-sealed stopcocks (Normag) were used for the sampling. The samples were first shipped to the institute that operated the station, where mixing ratios of H_2 and other trace gases were measured. H_2 mixing ratios were determined with reduction gas analysers, either the RGA-3 (Trace Analytics Inc.) or the Peak Performer 1 RCP (Peak Laboratories) (Hammer and Levin, 2009; Yver et al., 2009). Reduction gas analysers separate reduced gases such as H_2 from the air matrix by gas chromatography, and then quantify them via a redox reaction with mercuric oxide and detection of the resulting mercury vapour by UV absorption. We give mixing ratios in units of "parts per billion" (ppb) because this has become customary in atmospheric hydrogen research. This unit is equivalent to the SI-unit "nmole mole^{-1}". All laboratories used laboratory working standards that are now on the MPI2009 scale, developed at the MPI-BGC (Jordan and Steinberg, 2010). The samples were then shipped to the isotope laboratory at the Institute for Marine and Atmospheric Research (IMAU) of Utrecht University.

ACPD
11, 10087–10120, 2011

Typically, several months passed between sample collection and isotope analysis. A total of 480 flasks were analysed; the number of samples per station is listed in Table 2.

In Utrecht, a gas chromatography isotope-ratio mass spectrometry (GC-IRMS) system as described in Rhee et al. (2004) is used to separate H_2 from the air matrix and to determine its isotopic composition in a four-step procedure, as follows:

- A ≈750 ml glass sample volume is filled with sample air until pressure in the volume has reached ≈700 mbar. This sample air is then exposed to a Cold Head cooled by a liquid helium compressor to ≈40 K, so that all except the most volatile gases (H_2, He and Ne) condense.
- The remaining volatile gases are flushed with He carrier gas to a pre-concentration trap, consisting of a 1/8 inch (3.2 mm) stainless steel tube filled with 5 Å molecular sieve, immersed in liquid nitrogen, which is cooled down to the triple point of nitrogen (63 K) by pumping off the gas phase.
- After pre-concentration the trap is lifted from the liquid nitrogen and the trapped gases are flushed to a cryo-focus trap. This trap consists of a molsieve 5 Å capillary column, jacketed in a stainless steel tube and immersed in liquid nitrogen at ambient pressure (77 K). After focussing, the trap is lifted from the liquid nitrogen and the gases are injected into a 5 Å molsieve Gas Chromatography column kept in an oven at 50 °C, where the H_2 is separated from any potential contaminants.
- The purified H_2 is then injected through an open split system into the IRMS (ThermoFinnigan Delta plus XL) for determination of the D/H ratio.

In the IRMS chromatogram, the sample peak is typically bracketed by seven H_2 laboratory working gas peaks of pure H_2 before and two H_2 working gas peaks after. Following the same procedure as for the samples, comparable quantities of air from laboratory reference air bottles were typically measured twice a day. $m(H_2)$ in the laboratory reference bottle that was in use from March 2007 until February 2010 was determined by UHEI-IUP to be (546.2 ± 2.5) ppb, later confirmed by MPI-BGC to be

ACPD
11, 10087–10120, 2011

(545.0 ± 0.5) ppb. Its δ(D) ((+ 71.4 ± 2.0)‰, where the error bar indicates one standard error from 4 different determinations) was calculated using mixtures of synthetic air with H_2 of known isotopic composition ((−9.5 ± 0.5)‰ and (+205 ± 2)‰, certified by Messer Griesheim, Germany) that were measured on the GC-IRMS system on the same days as the laboratory reference bottle.

When this laboratory reference air bottle became exhausted, it was replaced with two other mixtures of synthetic air and H_2 ((580.78 ± 0.03) ppb and (244.3 ± 0.8) ppb, as determined by BGC Jena) that were regularly measured from December 2008 onward. From measurements during the overlap period, the isotopic composition of these new reference gases was calibrated versus the old reference air bottle ((+205.6 ± 0.3)‰ and (+196.8 ± 0.5)‰). Inspection of these measurements also allowed a robust assessment of the reproducibility of our system yielding a standard deviation of 4.5‰ in δ(D). A blank measurement was usually performed once a day as well. The blank peak area was usually less than 4% of a typical sample peak area.

The measurements of the laboratory reference bottles were used to construct 5-day moving average values of measured δ(D) values and the deviation of the measured from the assigned isotope value for each measurement day. These values were used to calculate the δ(D) values from the measurements of the samples. The moving average of the laboratory reference bottle measurements was replaced by the average of an adjusted selection of these measurements for some days where a relatively sudden shift in the measured values seemed to occur around these measurement days. An empirically determined factor (1.064) was used to correct for scale contraction of the isotope measurements.

The laboratory reference bottle measurements were used to calculate $m(H_2)$ for the samples as well. Mixing ratios determined by GC-IRMS measurement typically deviated less than 4% from the determinations by RGA-3 or Peak Performer. They were used for quality assessment of the data, but are not considered further in this paper.

Despite these calibration measures, δ(D) measurements from June 2010 onwards seemed to have a positive offset with respect to the previously measured samples and

ACPD
11, 10087–10120, 2011

an increased scatter. By comparing the respective samples from stations with long data series (Alert and Neumayer) with measurements from previous years, the offset could be empirically determined to be on average 9.7‰. Unfortunately, it could not be determined whether the offset was caused by simultaneous drift in the two laboratory reference bottles in use at that time or by the replacement of parts of the setup. At present the system is undergoing substantial rebuilding and further automation in order to be able to accommodate more reference gas measurements in the future.

The affected measurements of Alert and Neumayer samples still showed the same seasonal patterns as the previous measurements, and were therefore adjusted to fall on the same scale as the previous data by subtracting the empirically determined offset of 9.7‰. The respective data are indicated with open symbols in Fig. 2. Cape Verde samples that were also measured during this period showed a more erratic behaviour and were therefore omitted from the time series presented here. The Schauinsland samples after sept 2009 showed strong pollution signatures (high mixing ratios, as determined by both RGA-3 and GC-IRMS measurements, and very low δ(D) values), which coincided with CO_2 contaminations. As a leak or contamination in the sampling system was suspected, these data were omitted.

On visual inspection, some clear outliers in the individual time series were identified. These datapoints are indicated with open stars in Fig. 2. The δ(D) data that are indicated with open symbols in Fig. 2 were not used in further calculations.

3 Results and discussion

3.1 Time series

The time series of $m(H_2)$ and δ(D) for all six stations are shown in Fig. 2, and will be discussed individually in the following subsections. Figure 3 shows the seasonal averages from which an annual average was calculated for each station. Using the seasonal averages rather than the raw data for calculation of the mean has the advantage that

ACPD
11, 10087–10120, 2011

each of the seasons (DJF, MAM, JJA, SON) has equal weight, which avoids bias from having more samples from some seasons than from others.

Least-squares harmonic fits, with the function defined as:

$$y = a\cos(2\pi(x-\varphi)) + m \quad (2)$$

where x is the time in years and a, φ and m the fitting parameters, were made to the $m(H_2)$ and $\delta(D)$ data of the three stations that showed the clearest seasonal cycles in $\delta(D)$. These fits yielded the fitting parameters given in Table 3, and were used to construct the ellipses in the phase diagrams in Fig. 6.

3.1.1 Alert

Alert is the station with the largest number of analysed samples (Table 2) and about four full seasonal cycles of data. The annual average values are $m(H_2) = (496.9 \pm 1.2)$ ppb, and $\delta(D) = (122.8 \pm 0.5)$‰, where the error bar indicates the standard error of the mean (the standard deviation as a result of the variance in the measurements, divided by the square root of the number of measurements). A difference of 131 ppb is found between the highest and lowest $m(H_2)$ value, as well as a difference of 41‰ between the highest and lowest $\delta(D)$ (excluding the measurements affected by the 9.7‰ offset and outliers for $\delta(D)$).

A distinct seasonal cycle is observed for both $m(H_2)$ and $\delta(D)$ (Fig. 2) and $m(H_2)$ and $\delta(D)$ clearly increase and decrease out-of-phase. This out-of-phase timing appears as a result of the regional balance of sources and sinks, which is a combination of deuterium-depleted sources and the deuterium-enriching removal processes: in winter, H_2 accumulates from depleted sources (mainly combustion), leading to an H_2 peak and a $\delta(D)$ minimum in spring, while during summer, the removal processes are strong and the remaining H_2 becomes enriched, leading to an H_2 minimum and $\delta(D)$ maximum in autumn. The detailed study of the global H_2 isotope budget with the TM5 model (Pieterse et al., 2011) shows that the soil sink contributes most to the seasonal cycle of the mixing ratio, while the smaller photochemical sink has a larger effect on the isotopic

ACPD
11, 10087–10120, 2011

composition, due to the larger isotope fractionation. The dataset from Alert shows a similar seasonal behaviour as Rhee et al. (2006b) observed for NH near-tropopause averages of $m(H_2)$ and δ(D) obtained from three flights with a passenger aircraft.

The phase of the least-square harmonic fits to the Alert $m(H_2)$ data (Table 3) is similar to the phase reported by Rhee et al. (2006b), whereas the phase found for the δ(D) cycle is slightly different (the Alert δ(D)-cycle is slightly ahead of the (Rhee et al., 2006b) cycle). The average mixing ratio is lower. The most striking difference is in the amplitudes; the amplitudes of the seasonal cycles found at Alert are larger than for the Rhee et al. (2006b) NH near-tropopause averages, even more so since on visual inspection the harmonic fit seems to underestimate the amplitudes. The latter two differences can likely be attributed to the larger seasonality in the sinks at higher NH latitudes, due to the larger relative importance of the soil sink and the seasonal snow cover variation that modulates this sink. As we will show below, for the high-latitude NH stations, soil uptake dominates the seasonal cycle more than at lower NH latitudes. It seemingly also dominates the seasonal cycle more than for the NH high troposphere average. In a modelling study that focused on H_2 uptake by soil, Yashiro et al. (2011) found that the soil uptake flux for the latitude range north of 45° N has a much larger seasonal variation than for the 15° N to 45° N latitude range, which is in accordance with this finding. However, it should be noted that the analysis of Rhee et al. (2006b) is based on fitting a harmonic function to three data points only, whereas the Alert data series clearly captures the full seasonal evolution of the isotope signal.

Six δ(D) measurements on samples from another high northern latitude station, Point Barrow, Alaska, collected in the period from February to August 1997 have been published (Gerst and Quay, 2000). Unexpectedly, the δ(D) values of (+92 ± 10)‰, (one standard deviation) at Point Barrow are significantly lower than what we find at Alert and other NH stations (see below). The reason for this discrepancy is not understood, and the TM5 model (Pieterse et al., 2011) does not predict such a large difference either. It should be noted, however, that in-cylinder growth of H_2 is an issue in the early data from Gerst and Quay (2000). Specifically, four other samples from Point Barrow in

ACPD
11, 10087–10120, 2011

the study from Gerst and Quay (2000) were considered contaminated since their mixing ratios were different by more than 3σ from a multi-year average of NOAA-CMDL data. All samples were measured more than one year after collection and the discrepancy to the new values from Alert may indicate that the six samples considered reliable may have been contaminated too. The isotopic composition of the cylinder grown contamination was determined by (Gerst and Quay, 2000) to be $\delta(\mathrm{D}) = -614‰$, and thus only a few % of contamination from this source could lead to the observed depletions.

3.1.2 Mace Head

The time series for Mace Head spans more than three years now. The maximum amplitudes are 72 ppb and 34‰ for $m(H_2)$ and $\delta(\mathrm{D})$, respectively and the annual averages are (518.3 ± 1.4) ppb and (119.8 ± 0.7)‰. $m(H_2)$ shows a clear seasonal cycle; it increases steadily from autumn until summer, and then decreases rapidly. The $\delta(\mathrm{D})$ time series in 2007 and 2008 shows a minimum in late spring or early summer, indicating a seasonal cycle in $\delta(\mathrm{D})$ at Mace Head, which is also predicted by the TM5 model (Pieterse et al., 2011). In general, the $\delta(\mathrm{D})$ cycle moves in antiphase to the mixing ratio cycle as in Alert. However, it can be seen from the seasonal averages (Fig. 3), as well as from the phase obtained from the harmonic fit (Table 3), that the timing of the minimum is delayed with respect to Alert. The phase obtained from the harmonic fit to the Mace Head $\delta(\mathrm{D})$ data is in fact closer to the phase found by Rhee et al. (2006b) than from the fit to the Alert data. Still, as in Alert, the amplitude is larger than that from Rhee et al. (2006b). Mace Head can still be considered to be in the higher latitude part of the NH (especially since it receives much air from regions to the North-West, see below), and this large seasonal variation can thus be attributed to the large seasonal variation in the soil uptake flux at high NH latitudes as well. That this isotopic seasonal cycle is not visible in the first year of the series (2006) may be due to the small number of samples in this year. In 2009, there is one high $\delta(\mathrm{D})$ outlier right in the seasonal minimum. The $\delta(\mathrm{D})$ seasonal cycles vary considerably between 2007 and 2009, but the same is true for $m(H_2)$, so what causes interannual variations in $m(H_2)$ likely causes interannual signals in $\delta(\mathrm{D})$.

ACPD
11, 10087–10120, 2011

To investigate the origin of the interannual variations, backward trajectories were calculated with the NOAA HYSPLIT model to investigate if the rather high $m(H_2)$ and low δ(D) values in summer 2007 might have been a result of synoptic conditions that brought more locally polluted air than usual to the station. Such an effect was not found. The trajectories showed that most air masses that arrive at Mace Head come from the north Atlantic and the NH northern temperate to boreal regions to the west, and air masses that were sampled in summer 2007 were no exception. Grant et al. (2010) also showed that Mace Head rarely receives air masses from southerly latitudes, supporting the trajectory study. Therefore, transport of H_2-rich and δ(D)-depleted air from more southerly latitudes does not seem a very likely explanation. It is more likely that the full variability in H_2 cannot be seen at this station due to the limited time interval over which samples have been taken so far.

3.1.3 Schauinsland

In the time series from Schauinsland station, the maximum differences are 70 ppb and 45‰, and the seasonally weighted average values are (524.2 ± 0.9) ppb and (115.7 ± 0.9)‰. This is relatively similar to the values from Mace Head, but the seasonal cycles show differences. At Schauinsland, a clear seasonal cycle is visible in the $m(H_2)$ data, but not in the δ(D) data. In 2007, the δ(D) signal seems to trend downward, while in 2008 and 2009 it appears to trend upward. These trends are not statistically significant, though, but they underline that no clear seasonal cycle in δ(D) is present at Schauinsland.

Unlike Alert and Mace Head, Schauinsland is not a coastal but a continental location, close to anthropogenic sources, especially in the Rhine valley, and also regionally affected by the soil sink. Possibly, significant nitrogen fixation by soil microbes takes place in the surrounding region as well. H_2 produced by nitrogen fixers has a very depleted source signature (Table 1), so only a small amount of this H_2 may have a significant effect on the isotopic signature of the total ambient H_2. The station is usually above the boundary layer at night, and within the boundary layer during the day,

ACPD
11, 10087–10120, 2011

particularly in summer (Schmidt et al., 1996). The upper edge of the boundary layer generally passes the station altitude after 10:00 a.m., so samples collected after this time are potentially locally influenced; they may contain boundary layer air that has been in contact with local (anthropogenic) sources and the surface. Most of the samples analyzed for this record were sampled before 10:00 a.m.; about 10% was collected later in the day. However, excluding these samples from the time series did not yield a more distinct seasonal cycle. This indicates that the deviations in the isotopic composition are not a product of local factors only. It should be noted that also the TM5 model predicts a considerably smaller seasonal cycle in δ(D) for Schauinsland compared to Mace Head (Pieterse et al., 2011), so a longer time series may be needed to clearly distinguish the cycle from the data scatter.

3.1.4 Cape Verde

Although the Cape Verde time series is the shortest (little more than one year), the data indicate a clearer seasonal cycle than for Mace Head. As in Alert and Mace Head, $m(H_2)$ and δ(D) vary out-of-phase. The timing of the minima and maxima is closer to what is observed at Mace Head than at Alert. The mixing ratio peaked at 567 ppb in August and then decreased by 57 ppb to 510 ppb at the end of the year. From April until August the δ(D) value was rather constant (minimum value of 99‰ in July) and after August it increased until the end of the year (maximum observed value 136‰ in November). Seasonally weighted annual averages of (538.8 ± 1.4) ppb and (118.4 ± 1.1)‰ were observed. The amplitude found with the harmonic fit to the data is remarkably large, larger than for Mace Head and Alert. This is in contrast to the TM5 model results (Pieterse et al., 2011) where the seasonal variation in δ(D) at Cape Verde is somewhat smaller than for Mace Head and Alert. The harmonic fit does not seem to underestimate the amplitudes as it does for the Alert and Mace Head datasets, but at these stations this was largely due to interannual differences, which are not relevant for Cape Verde (yet).

ACPD
11, 10087–10120, 2011

3.1.5 Amsterdam Island

The time series from Amsterdam Island does not show a very distinct seasonal cycle. H_2 mixing ratios only vary between 535 and 570 ppb and no clear seasonal signal can be identified in the δ(D) data. Some unexplained extreme outliers do occur in the measurements. Excluding these outliers, the maximal variability in mixing ratio is 28 ppb, and in the isotopic composition 32‰. The yearly average values are (549.5 ± 0.6) ppb and (142.3 ± 1.0)‰.

3.1.6 Neumayer

At present, the Neumayer time series covers 5 full seasonal cycles, and average values are (551.1 ± 0.4) ppb and (148.4 ± 0.4)‰. A clear seasonal variation can be distinguished in the mixing ratio data, but not in the isotope data. The mixing ratios vary by at most 30 ppb over the year, and the isotope values by at most 28‰, making Neumayer the station with the lowest variability in δ(D). A relatively sharp "dip" was first detected in the δ(D) values at the end of 2005. This feature was not observed in the other years, so we suspect that this is an artefact rather than a real atmospheric signal and flagged these datapoints as outliers.

The variation in δ(D) in Neumayer is remarkably small, considering that $m(H_2)$ does show a clear cycle. There is a hydrogen maximum in austral summer, likely an effect of photochemical production, but this does not effect δ(D) since the isotopic composition of H_2 from photochemical production is only slightly enriched with respect to the atmospheric reservoir (Price et al., 2007; Pieterse et al., 2009, 2011) . The sink processes also have an enriching effect on the remaining H_2 reservoir (Talukdar et al., 1996; Gerst and Quay, 2001; Rahn et al., 2002a). The TM5 model study from Pieterse et al. (2011) indicates that horizontal transport of deuterium-depleted H_2 from lower latitudes could be an important factor in the seasonality of δ(D) at high southern latitudes and could compensate the enriching effects.

ACPD
11, 10087–10120, 2011

3.1.7 Seasonal mean variations

Averages per season (DJF, MAM,JJA and SON) were calculated for each station and are shown in Fig. 3. This averaging eliminates the scatter from analytical uncertainty and short-term natural variability and allows the general shape of the seasonal cycles to be compared between the stations. The anticorrelated seasonal cycles of δ(D) and $m(H_2)$ at Alert can be seen very clearly. There is also an anticorrelation at Mace Head and Cape Verde, but the timing of the minima and maxima is different from the timing at Alert. Although it was not visible in the raw data in Fig. 2, the seasonal averages of the Schauinsland data seem to show a weak anticorrelation, which is primarily caused by the δ(D) value having a minimum in spring, when $m(H_2)$ shows a maximum. In contrast to the NH stations, the two SH stations have a very small seasonal cycle in $m(H_2)$ and δ(D). The δ(D) cycle at Neumayer does not seem correlated to the δ(D) cycle at Amsterdam Island.

3.2 Latitudinal gradients

Figure 4 shows the latitudinal dependence of the seasonal averages. In all seasons, both mixing ratios and δ(D) values are higher in the SH than in the NH. The lowest average mixing ratios are found for the highest-latitude NH station (Alert) in all seasons. The minimum in δ(D) is, however, not found at Alert for any season, but either at one of the midlatitude stations, or, in summer (JJA), at Cape Verde. As anthropogenic H_2 emissions originate mainly from temperate latitudes, which is a clear feature in H_2 emission estimates used in recent modelling studies (Hauglustaine and Ehhalt, 2002; Price et al., 2007), and H_2 from anthropogenic sources is usually depleted with respect to the atmospheric H_2, the midlatitude minimum can be attributed to anthropogenic influence. This is also evident in the spatial δ(D) distribution modelled in TM5 (Pieterse et al., 2011).

Gerst and Quay (2000) concluded from their dataset, obtained from an Atlantic Transect at the end of 1998 and two stations in North America, that there was a poleward decrease in δ(D). However, at their northernmost sampling point (Point Barrow, 71° N),

ACPD
11, 10087–10120, 2011

δ(D) values seem to be exceptionally low. Whereas the rest of the data agree reasonably well with our measurements, their measurements from Point Barrow are more than 20‰ lower than our data from Alert. The potential problems with these Point Barrow measurements have been discussed above. We note that without this sampling point, also the data from Gerst and Quay (2000) show a δ(D) minimum at temperate northern latitudes.

From Fig. 4, it is clear that the latitudinal gradient varies with season. As the seasonal variation in both $m(H_2)$ and δ(D) is much larger in the NH than in the SH, the size of the latitudinal gradient is for the largest part determined by the variation in the NH. Hence, the smallest pole-to-pole δ(D) difference (19 ‰ between Neumayer and Alert) is found when δ(D) is at its maximum in Alert, i.e., in SON. During this season, $m(H_2)$ is lowest in Alert, and therefore the $m(H_2)$ difference is largest (72 ppb). At that time, soil uptake in Alert is past its summer peak, so that H_2 mixing ratios are low and the remaining H_2 is isotopically enriched. Reversely, the largest δ(D) pole-to-pole difference (34‰) is found when δ(D) is at its minimum in Alert and $m(H_2)$ is at its maximum, namely in MAM, when over winter H_2 from depleted sources has accumulated without being absorbed by the snow-covered soil. This is accompanied by the smallest difference in $m(H_2)$ (35 ppb).

The interhemispheric difference reported by Gerst and Quay (2000) was about 15‰, and Rice et al. (2010) found a similar gradient, (16 ± 12)‰. The interpolar difference from the EUROHYDROS stations is clearly larger, but we miss a station at low southern latitudes to be able to make a reliable southern hemispheric budget.

3.3 Latitude dependence of the apparent fractionation factor

In cases where the seasonal cycle of H_2 and its isotopic composition is primarily determined by the sink processes, the fractionation factor α, i.e., the ratio of the removal rate of the heavy isotope species (k_{HD}) to the removal rate of the light isotope species (k_{HH}), can be calculated from a time series as a single stage Rayleigh fractionation process (see Rhee et al., 2006b). In such a Rayleigh removal process, $m(H_2)$ and δ(D) evolve as

ACPD
11, 10087–10120, 2011

$$(\alpha - 1)\ln\left[\frac{m(H_2)}{m(H_2,\max)}\right] = \ln[\delta(D) + 1] + c \quad (3)$$

where $m(H_2, \max)$ is the maximum value for $m(H_2)$ found in the series and c is a constant. The real situation at the measurement stations is more complex than this simple Rayleigh fractionation model, as will be discussed below. Still, the apparent fractionation factor α_{app} was calculated for each station from the slope of a linear fit to the data in a Rayleigh fractionation plot (Fig. 5). To make the straight-line fits, a Weighted Total Least-Squares (WTLS) fitting algorithm that was described by Krystek and Anton (2007) was used. This algorithm takes errors in both the x- and the y-direction into account. The squared correlation coefficient (R^2) and the F-test p-value were calculated for each station in the same way as they would be calculated for an "ordinary" least-squares fit of a straight line. The fits to the Amsterdam Island and Neumayer data yielded p-values below 0.05, suggesting a less than 95% significance of the correlation. The fit to the Schauinsland data did yield a p-value that was slightly larger than 0.05, but the R^2-value for this fit is very low, which indicates that only a very small part of the variation present in the dataset is described by the fit. This means that the simple Rayleigh fractionation model may not be adequate for evaluation of the time series from Schauinsland and the SH. This is not surprising, considering that no clear isotope seasonal cycles were found for these stations.

Of course, the isotopic composition of the H_2 at the measurement stations depends not only on the fractionation in the removal processes, but also on the isotopic composition of the sources that influence the sites and their variation over the year. Also the relative contribution of the two sink processes (atmospheric OH oxidation and uptake by soils) to the total sink could conceivably vary with season. In this light, it is illustrative to look at the phase diagrams (δ(D) plotted against $m(H_2)$) of the monthly means that can be constructed from the three stations that show clear cycles (Fig. 6). For Alert, it is clear that these points do not fall on a single straight fractionation line, but on the ellipse that is traced by the two harmonic functions that were fitted to the $m(H_2)$ and δ(D) time series. This shows that in the fractionation plots in Fig. 5, not all of the spread

ACPD
11, 10087–10120, 2011

around the fractionation lines is random scatter; some of this spread is caused by the phase difference between the $m(H_2)$ and $\delta(D)$ seasonal cycles. The largest part of this phase difference is probably caused by seasonal variation in the sources and sinks.

Allan et al. (2001) described such phase ellipses for model results of methane mixing ratio and the carbon isotopic composition of methane ($\delta(^{13}C,CH_4)$). In their simulations with only one source and a sink process, the monthly means fell on a straight line. This line broadened into an ellipse when different sources with different seasonal cycles were combined, with the largest broadening effect for the sources of which the isotopic signature differed the most from the isotopic signature of the mean source. However, the differing phases of the different sources did not appreciably affect the slope of the major axis of the ellipse: this slope depended robustly on the fractionation factor assumed for the sink, suggesting that even if the phase diagram shows a broadened ellipse, this slope can provide a good estimate of the fractionation in the sink. The ellipse major axis coincided largely with a relationship the authors termed the "KIE line" after the Kinetic Isotope Effect, which is described by:

$$\Delta\delta = \varepsilon(1+\delta_0)\Delta C/C_0 \quad (4)$$

with subscript zero indicating a mean value, Δ indicating the difference of a value from the mean, and $\varepsilon = \alpha - 1$.

In the case of H_2, seasonal variation in the sources and sinks contributes to the ellipse eccentricity, but Rhee et al. (2006b) showed that as long as the H_2 system is in isotopic equilibrium on an annual basis, the isotopic fractionation does not depend on seasonal changes in source emissions. Since there is no evidence for a trend in either $m(H_2)$ or $\delta(D)$, it is reasonable to assume isotope equilibrium for the years over which the data presented here were collected.

A factor that could still affect the analysis is a seasonally varying contribution of the two main sinks. However, especially in Alert, any variations in the relative contributions of the two sinks over the year are expected to be small, because even if soil uptake and atmospheric OH oxidation do not follow the exact same seasonal pattern, their patterns

ACPD
11, 10087–10120, 2011

are expected to share the main characteristics, with a minimum in winter, and a peak in summer. Hence, although the Rayleigh fractionation model does not represent the full complexity of reality at the stations, the apparent fractionation constants determined with this model provide a good estimate of the total sink fractionation.

For Alert, Mace Head and Cape Verde, KIE lines were calculated with the hydrogen α_{app} obtained for the different stations, as well as with the fractionation constants (Rhee et al., 2006b) for the two H_2 sink processes and added to Fig. 6. Clearly, for Alert and Mace Head the KIE line of the fit lies closest to the KIE line of soil uptake, whereas in Cape Verde it lies closest to atmospheric OH oxidation. For these three stations, α_{app} is plotted versus station latitude in Fig. 7a. The apparent fractionation factor can be interpreted as a combination of the fractionation factors in the main sink processes. For Alert and Mace Head, α_{app} is close to the fractionation factor assigned to soil uptake ($\alpha = 0.943 \pm 0.007$). Rhee et al. (2006b) also concluded from a similar analysis on a small set of upper tropospheric air samples that the seasonal cycle of H_2 in the NH is largely driven by soil uptake. Closer to the equator, at Cape Verde, α_{app} is lower, closer to the value for oxidation by the hydroxyl radical (OH) ($\alpha = 0.58 \pm 0.007$). This indicates that the relative importance of the uptake by soil with respect to the destruction by OH increases with latitude.

Figure 7b shows the relative contribution of both sinks processes to the total destruction of H_2, as can be calculated from these isotope data if α_{app} is assumed to be a simple mass weighted average of the fractionation factors of soil removal and reaction with OH. This calculation yields that OH destroys more than half of the H_2 at Cape Verde, but that at Alert, almost 90% of the H_2 is destroyed by soil uptake. In the TM5 model study, H_2 destruction is clearly dominated by the soil sink in the high northern latitude band (30° N–90° N), whereas the two sinks are of comparable magnitude in the tropical latitude band (30° N–30° S) (Fig. 8 in Pieterse et al., 2011).

ACPD
11, 10087–10120, 2011

4 Conclusions

Air samples from six EUROHYDROS stations have been analysed regularly for $m(H_2)$ and $\delta(D)$, which allows analysis of the temporal and latitudinal distribution of H_2 and its isotopic composition. These data greatly expand the existing $\delta(D)$ dataset, and can be used to constrain the global and regional H_2 budgets with the help of global and regional models.

The out-of-phase behaviour of $m(H_2)$ and $\delta(D)$ that was proposed for the NH (Rhee et al., 2006b) is seen at Mace Head and Cape Verde, and particularly clearly at Alert, but not at Schauinsland, which is a more continental station and closer to anthropogenic source regions. The SH stations show very little variation in $\delta(D)$, even when $m(H_2)$ exhibits a small seasonal cycle. The $\delta(D)$ data show a clear latitudinal gradient with higher values in the SH than in the NH. This gradient varies with season, mainly driven by the seasonality in the NH. The observed pole-to-pole differences are larger than observed on ship cruises (Gerst and Quay, 2000; Rice et al., 2010). The $\delta(D)$ minimum is not found at the highest NH latitude station, but at lower NH latitudes, where the influence of anthropogenic combustion sources is strongest. Assuming that the seasonality of the $m(H_2)$ and $\delta(D)$ time series is mainly determined by the removal processes, the relative changes of $m(H_2)$ and $\delta(D)$ can be used to provide information on the relative sink strengths of soil deposition and atmospheric oxidation. The data then confirm that at high northern latitudes, the removal processes are almost completely dominated by deposition to soil, whereas in the tropics, soil deposition and atmospheric oxidation are of similar importance.

Acknowledgements. This project was part of the EUROHYDROS project, funded via the Sixth Framework Programme of the European Union (SUSTDEV-2005-3.I.2.1 Atmospheric composition change: Methane, Nitrous Oxide and Hydrogen). We also acknowledge support from the Dutch NWO-ACTS project 053.61.026.

For the trajectory study of the Mace Head data we used the NOAA Air Resources Laboratory (ARL) Hybrid Single Particle Lagrangian Integrated Trajectory Model (HYSPLIT): http://www.

arl.noaa.gov/HYSPLIT_info.php. Graphics for this article were generated using Python 2.6 with the matplotlib and pylab packages.

References

Allan, W., Manning, M., Lassey, K., Lowe, D. and Gomez, A. Modeling the variation of $\delta^{13}C$ in atmospheric methane: Phase ellipses and the kinetic isotope effect, Glob. Biochem. Cy., 15(2), 467–481, doi:10.1029/2000GB001281, 2001.

Ehhalt, D. H.: Tritium and deuterium in atmospheric hydrogen, Tellus, 18(2–3), 249–255, doi:10.1111/j.2153-3490.1966.tb00233.x, 1966.

Ehhalt, D. H. and Rohrer, F. The tropospheric cycle of H_2: a critical review, Tellus B, 61(3), 500–535, doi:10.1111/j.1600-0889.2009.00416.x, 2009.

Ehhalt, D. H., Schmidt, U., and Heidt, L. E. Vertical Profiles of Molecular Hydrogen in the Troposphere and Stratosphere, J. Geophys. Res., 82(37), 5907–5911, doi:10.1029/JC082i037p05907, 1977.

Engel, A.: EUROHYDROS, A European Network for Atmospheric Hydrogen Observations and studies: Final Report, 2009.

Feck, T., Grooß, J.-U., and Riese, M. Sensitivity of Arctic ozone loss to stratospheric H_2O, Geophys. Res. Lett., 35(1), 1–20, doi:10.1029/2007GL031334, 2008.

Feilberg, K. L., Johnson, M. S., Bacak, A., Röckmann, T. and Nielsen, C. J. Relative tropospheric photolysis rates of HCHO and HCDO measured at the European Photoreactor Facility., J. Phys. Chem. A, 111(37), 9034–46, doi:10.1021/jp070185x, 2007.

Gerst, S. and Quay, P. The deuterium content of atmospheric molecular hydrogen: Method and initial measurements, J. Geophys. Res., 105, 26433–26445, doi:10.1029/2000JD900387, 2000.

Gerst, S. and Quay, P. Deuterium component of the global molecular hydrogen cycle, J. Geophys. Res., 106, 5021–5031, doi:10.1029/2000JD900593, 2001.

Glueckauf, E. and Kitt, G. P. The hydrogen content of atmospheric air at ground level, Q. J. Roy. Meteorol. Soc., 83(358), 522–528, doi:10.1002/qj.49708335808, 1957.

Grant, A., Witham, C. S., Simmonds, P. G., Manning, A. J., and O'Doherty, S.: A 15 year record of high-frequency, in situ measurements of hydrogen at Mace Head, Ireland, Atmos. Chem. Phys., 10, 1203–1214, doi:10.5194/acp-10-1203-2010, 2010.

ACPD
11, 10087–10120, 2011

Hammer, S. and Levin, I.: Seasonal variation of the molecular hydrogen uptake by soils inferred from continuous atmospheric observations in Heidelberg, southwest Germany, Tellus B, 61(3), 556–565, doi:10.1111/j.1600-0889.2009.00417.x, 2009.

Hauglustaine, D. A. and Ehhalt, D. H. A three-dimensional model of molecular hydrogen in the troposphere, J. Geophys. Res., 107, 4330, doi:10.1029/2001JD001156, 2002.

Jordan, A. and Steinberg, B.: Calibration of atmospheric hydrogen measurements, Atmos. Meas. Tech., 4, 509–521, doi:10.5194/amt-4-509-2011, 2011.

Krystek, M. and Anton, M. A weighted total least-squares algorithm for fitting a straight line, Meas. Sci. Technol., 18(11), 3438–3442, doi:10.1088/0957-0233/18/11/025, 2007.

Nilsson, E. J. K., Johnson, M. S., Taketani, F., Matsumi, Y., Hurley, M. D., and Wallington, T. J.: Atmospheric deuterium fractionation: HCHO and HCDO yields in the $CH_2DO + O_2$ reaction, Atmos. Chem. Phys., 7, 5873–5881, doi:10.5194/acp-7-5873-2007, 2007.

Novelli, P. C., Lang, P. M., Masarie, K. A., Hurst, D. F., Myers, R., and Elkins, J. W. Molecular hydrogen in the troposphere: Global distribution and budget, J. Geophys. Res., 104, 30427–30444, doi:10.1029/1999JD900788, 1999.

Pieterse, G., Krol, M. C., and Röckmann, T.: A consistent molecular hydrogen isotope chemistry scheme based on an independent bond approximation, Atmos. Chem. Phys., 9, 8503–8529, doi:10.5194/acp-9-8503-2009, 2009.

Pieterse, G., Krol, M. C., Batenburg, A. M., Steele, L. P., Krummel, P. B., Langenfelds, R. L., and Röckmann, T.: Global modelling of H_2 mixing ratios and isotopic compositions with the TM5 model, Atmos. Chem. Phys. Discuss., 11, 5811–5866, doi:10.5194/acpd-11-5811-2011, 2011.

Price, H., Jaeglé, L., Rice, A., Quay, P., Novelli, P. C., and Gammon, R.: Global budget of molecular hydrogen and its deuterium content: Constraints from ground station, cruise, and aircraft observations, J. Geophys. Res., 112(D22), 1–16, doi:10.1029/2006JD008152, 2007.

Rahn, T., Eiler, J. M., Kitchen, N., Fessenden, J. E., and Randerson, J. T.: Concentration and δD of molecular hydrogen in boreal forests: Ecosystem-scale systematics of atmospheric H_2, Geophys. Res. Lett., 29(18), 1888, doi:10.1029/2002GL015118, 2002a.

Rahn, T., Kitchen, N., and Eiler, J. D/H ratios of atmospheric H_2 in urban air: results using new methods for analysis of nano-molar H_2 samples, Geochim. Cosmochim. Ac., 66(14), 2475–2481, doi:10.1016/S0016-7037(02)00858-X, 2002b.

Rahn, T., Eiler, J. M., Boering, K. A., Wennberg, P. O., McCarthy, M. C., Tyler, S., Schauffler, S., Donnelly, S., and Atlas, E. Extreme deuterium enrichment in stratospheric hydrogen and the

ACPD
11, 10087–10120, 2011

global atmospheric budget of H2, Nature, 424, 918–921, doi:10.1038/nature01917, 2003.
Rhee, T. S., Mak, J., Röckmann, T., and Brenninkmeijer, C. A. M. Continuous-flow isotope analysis of the deuterium/hydrogen ratio in atmospheric hydrogen, Rapid Commun. Mass Spectrom., 18(3), 299–306, doi:10.1002/rcm.1309, 2004.
Rhee, T. S., Brenninkmeijer, C. A. M., Brass, M. and Brühl, C. Isotopic composition of H_2 from CH_4 oxidation in the stratosphere and the troposphere, J. Geophys. Res., 111(D23), D23303, doi:10.1029/2005JD006760, 2006a.
Rhee, T. S., Brenninkmeijer, C. A. M., and Röckmann, T.: The overwhelming role of soils in the global atmospheric hydrogen cycle, Atmos. Chem. Phys., 6, 1611–1625, doi:10.5194/acp-6-1611-2006, 2006b.
Rhee, T. S., Brenninkmeijer, C. A. M., and Röckmann, T.: Hydrogen isotope fractionation in the photolysis of formaldehyde, Atmos. Chem. Phys., 8, 1353–1366, doi:10.5194/acp-8-1353-2008, 2008.
Rice, A., Quay, P., Stutsman, J., Gammon, R., Price, H., and Jaeglé, L. Meridional distribution of molecular hydrogen and its deuterium content in the atmosphere, J. Geophys. Res., 115(D12), 1–12, doi:10.1029/2009JD012529, 2010.
Röckmann, T., Rhee, T. S., and Engel, A.: Heavy hydrogen in the stratosphere, Atmos. Chem. Phys., 3, 2015–2023, doi:10.5194/acp-3-2015-2003, 2003.
Röckmann, T., Álvarez, C. X. G., Walter, S., Veen, C. van der, Wollny, A. G., Gunthe, S. S., Helas, G., Pöschl, U., Keppler, F., Greule, M., and Brand, W. A. Isotopic composition of H_2 from wood burning: Dependency on combustion efficiency, moisture content, and δD of local precipitation, J. Geophys. Res., 115, D17308, doi:201010.1029/2009JD013188, 2010a.
Röckmann, T., Walter, S., Bohn, B., Wegener, R., Spahn, H., Brauers, T., Tillmann, R., Schlosser, E., Koppmann, R., and Rohrer, F.: Isotope effect in the formation of H_2 from H_2CO studied at the atmospheric simulation chamber SAPHIR, Atmos. Chem. Phys., 10, 5343–5357, doi:10.5194/acp-10-5343-2010, 2010b.
Schmidt, M., Graul, R., Sartorius, H., and Levin, I. Carbon dioxide and methane in continental Europe: a climatology, and ^{222}Radon-based emission estimates, Tellus B, 48(4), 457–473, doi:10.1034/j.1600-0889.1994.t01-2-00002.x-i1, 1996.
Schmidt, U.: Molecular hydrogen in the atmosphere, Tellus, 26(1–2), 78–90, doi:10.1111/j.2153-3490.1974.tb01954.x, 1974.
Schmidt, U. and Seiler, W. A New Method for Recording Molecular Hydrogen in Atmospheric Air, J. Geophys. Res., 75(9), 1713–1716, doi:197010.1029/JC075i009p01713, 1970.

ACPD
11, 10087–10120, 2011

Schultz, M. G., Diehl, T., Brasseur, G. P., and Zittel, W. Air pollution and climate-forcing impacts of a global hydrogen economy, Science, 302(5645), 624–627, doi:10.1126/science.1089527, 2003.

Talukdar, R. K., Gierczak, T., Goldfarb, L., Rudich, Y., Rao, B. S. M., and Ravishankara, R.: Kinetics of Hydroxyl Radical Reactions with Isotopically Labeled Hydrogen, J. Phys. Chem., 100(8), 3037–3043, doi:10.1021/jp9518724, 1996.

Tromp, T. K., Shia, R.-L., Allen, M., Eiler, J. M., and Yung, Y. L. Potential Environmental Impact of a Hydrogen Economy on the Stratosphere, Science, 300, 1740–1742, 2003.

Vollmer, M. K., Walter, S., Bond, S. W., Soltic, P., and Röckmann, T.: Molecular hydrogen (H_2) emissions and their isotopic signatures (H/D) from a motor vehicle: implications on atmospheric H_2, Atmos. Chem. Phys., 10, 5707–5718, doi:10.5194/acp-10-5707-2010, 2010.

Warwick, N. J., Bekki, S., Nisbet, E. G., and Pyle, J. A.: Impact of a hydrogen economy on the stratosphere and troposphere studied in a 2-D model, Geophys. Res. Lett., 31(5), 2–5, doi:10.1029/2003GL019224, 2004.

Yashiro, H., Sudo, K., Yonemura, S., and Takigawa, M.: The impact of soil uptake on the global distribution of molecular hydrogen: chemical transport model simulation, Atmos. Chem. Phys. Discuss., 11, 4059–4103, doi:10.5194/acpd-11-4059-2011, 2011.

Yver, C., Schmidt, M., Bousquet, P., Zahorowski, W., and Ramonet, M.: Estimation of the molecular hydrogen soil uptake and traffic emissions at a suburban site near Paris through hydrogen, carbon monoxide, and radon-222 semicontinuous measurements, J. Geophys. Res., 114(D18), 1–12, doi:10.1029/2009JD012122, 2009.

ACPD

11, 10087–10120, 2011

Table 1. The global budget of atmospheric H_2, with source and sink strengths and isotopic signatures used by different authors.

	Novelli et al. (1999)	Rhee et al. (2006)		Price et al. (2007)		Ehhalt and Rohrer (2009)	Pieterse et al. (2011)	
Sources	Source strength (Tg H_2 a^{-1})	Source strength (Tg H_2 a^{-1})	Source signature (‰)	Source strength (Tg H_2 a^{-1})	Source signature (‰)	Source strength (Tg H_2 a^{-1})	Source strength (Tg H_2 a^{-1})	Source signature (‰)
Fossil fuel burning	15 ± 10	15 ± 6	−270	18.3	−196	11 ± 4	17.0^{+3}_{-6}	−196
Biomass burning	16 ± 5	16 ± 3	−90	10.1	−290	15 ± 6	15.0^{+5}_{-5}	−260
Biofuel				4.4	−290			
Ocean	3 ± 2	6 ± 5	−700	6	−628	6 ± 3	5.0^{+1}_{-2}	−628
Land N_2 fixation	3 ± 1	6 ± 5	−700	0		3 ± 2	3.0^{+3}_{-3}	−628
Methane oxidation	26 ± 9	64 ± 12 (incl. VOC)	+190	24.5	+162	23 ± 8	37.3	+116
VOC oxidation	14 ± 7			9.8	+162	18 ± 7		
Sinks	Sink strength (Tg H_2 a^{-1})	Sink strength (Tg H_2 a^{-1})	Sink fractionation factor (α=k_{HD}/k_{H2})	Sink strength (Tg H_2 a^{-1})	Sink fractionation factor (α=k_{HD}/k_{H2})	Sink strength (Tg H_2 a^{-1})	Sink strength (Tg H_2 a^{-1})	Sink fractionation factor (α=k_{HD}/k_{H2})
Uptake by soils	56 ± 41	88 ± 11	0.943 ± 0.007	55	0.943	60^{+30}_{-20}	55.8	0.925
Oxidation by OH	19 ± 5	19 ± 3	0.58 ± 0.07	18	0.568	19 ± 5	22.1	0.542

ACPD
11, 10087–10120, 2011

Table 2. The locations, operating institutes, length, average $m(H_2)$ and $\delta(D)$ values and maximum variations of the sample record presented here for the six EUROHYDROS stations.

Station	Coordinates	Operating Institute	Samples	Record length (months)	Average $m(H_2)$ (ppb)	Max. $m(H_2)$ variation	Average $\delta(D)$ (‰ vs. VSMOW)	Max. $\delta(D)$ variation
Alert	82.45° N 65.52° W	UHEI-IUP	194	47	496.9 ± 1.2	131	122.8 ± 0.5	41
Mace Head	53.20° N 9.54° W	LSCE	71	41	518.3 ± 1.4	72	119.8 ± 0.7	34
Schauinsland	47.55° N 7.54° E	UHEI-IUP	127	34	524.2 ± 0.9	70	115.7 ± 0.9	45
Cape Verde	13.6° N 22.6° W	MPI-BGC	42	12	538.8 ± 1.4	57	118.4 ± 1.1	37
Amsterdam Island	−37.57° S 77.32° E	LSCE	63	38	549.5 ± 0.6	28	142.3 ± 1.0	32
Neumayer	−70.39° S 8.15° W	UHEI-IUP	110	59	551.1 ± 0.4	30	148.4 ± 0.4	18

ACPD
11, 10087–10120, 2011

Table 3. The obtained fitting parameters for a least-square fit with a harmonic function to the data from Alert, Mace Head and Cape Verde ($y = a\cos(2\pi(x-\phi)) + m$).

	Alert		Mace Head		Cape Verde		(Rhee et al., 2006b) NH hemisphere average	
	$m(H_2)$ (ppb)	δ(D) (‰)	$m(H_2)$ (ppb)	δ(D) (‰)	$m(H_2)$ (ppb)	δ(D) (‰)	$m(H_2)$	δ(D)
Amplitude (a)	27.8 ± 1.4	7.5 ± 0.7	20.3 ± 1.9	7.0 ± 1.0	13.9 ± 2.0	12.1 ± 1.2	18.2 ± 1.6	4.0 ± 0.9
Phase (ϕ)	0.24 ± 0.01	0.66 ± 0.02	0.33 ± 0.01	0.83 ± 0.02	0.44 ± 0.02	0.94 ± 0.02	0.28 ± 0.01	0.85 ± 0.05
Average (m)	497.0 ± 1.0	122.8 ± 0.5	517.6 ± 1.3	120.2 ± 0.7	539.0 ± 1.3	118.2 ± 0.8	543.4 ± 0.8	128.3 ± 0.7

ACPD
11, 10087–10120, 2011

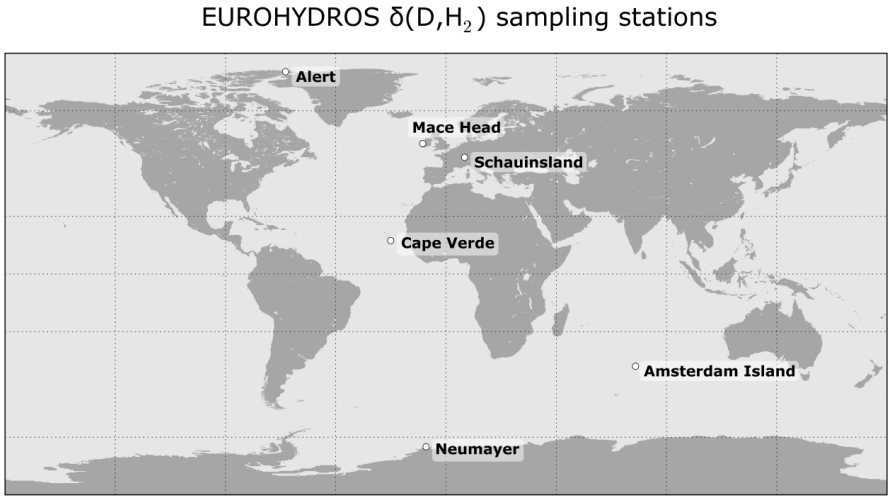

Fig. 1. The six EUROHYDROS stations that were used for δ(D) observations.

ACPD
11, 10087–10120, 2011

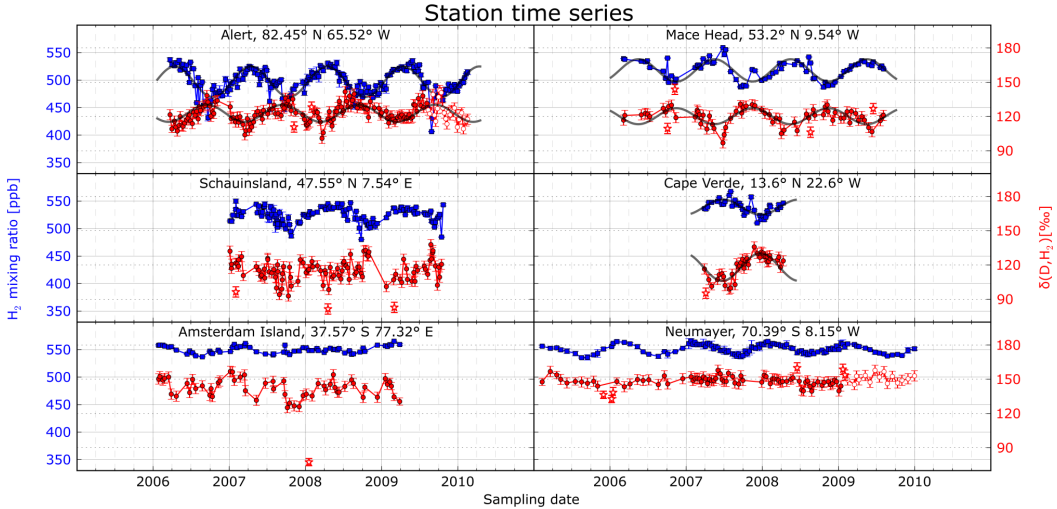

Fig. 2. $m(H_2)$ (blue squares, measured by UHEI-IUP, LSCE and MPI-BGC- Jena) and $\delta(D)$ (red circles) measured by IMAU on samples from the six stations. Solid grey lines represent a harmonic best fit to the data from Alert. Error bars indicate one standard deviation for $m(H_2)$ determined from successive measurements, and one standard error for $\delta(D)$ (the standard deviation of 4.5‰, as determined from repeated laboratory standard bottle measurements, divided by the square root of the number of repeat measurements of the same flask). Open red circles indicate the $\delta(D)$-values where an empirical value of 9.7‰ was subtracted to adjust for the bias that affected the GC-IRMS system from June 2010 onward. Open red stars indicate other unexplained outliers. None of the open-symbol data are used in any further calculations. Some outliers at Amsterdam Island are off the scale.

ACPD
11, 10087–10120, 2011

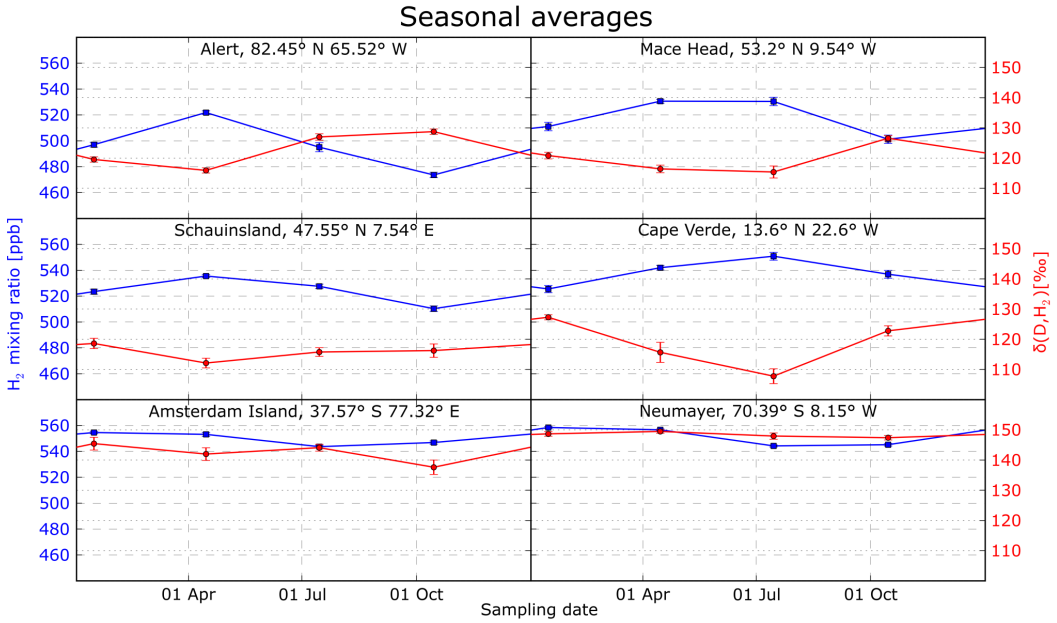

Fig. 3. Seasonal averages of $m(H_2)$ (UHEI, LSCE and BGC-Jena) and $\delta(D)$ (IMAU) plotted versus time of year. Error bars indicate one standard error, which is calculated purely from variance in the values obtained for one season.

ACPD
11, 10087–10120, 2011

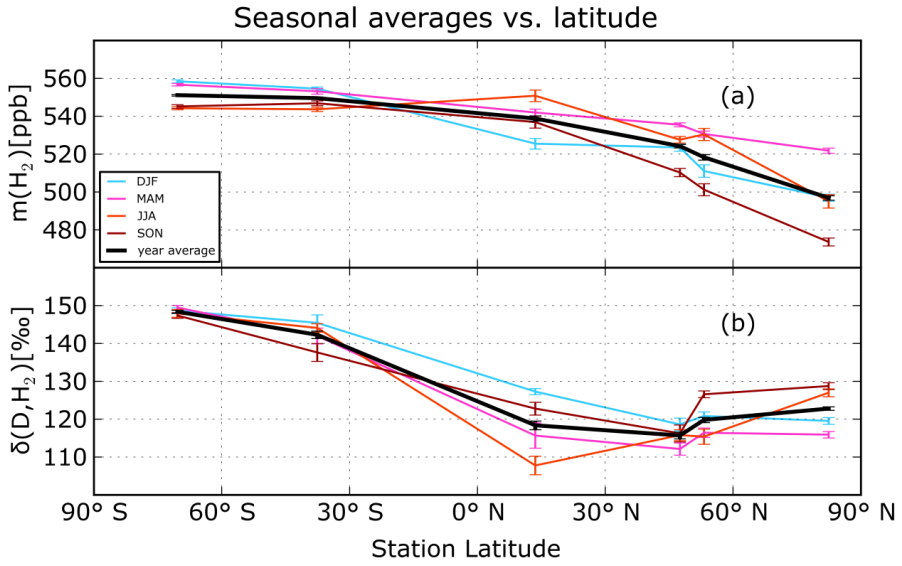

Fig. 4. Average H_2 mixing ratios **(a)** and δ(D) **(b)** per season and over the whole year at the different stations, plotted as a function of station latitude. Error bars indicate one standard error.

ACPD
11, 10087–10120, 2011

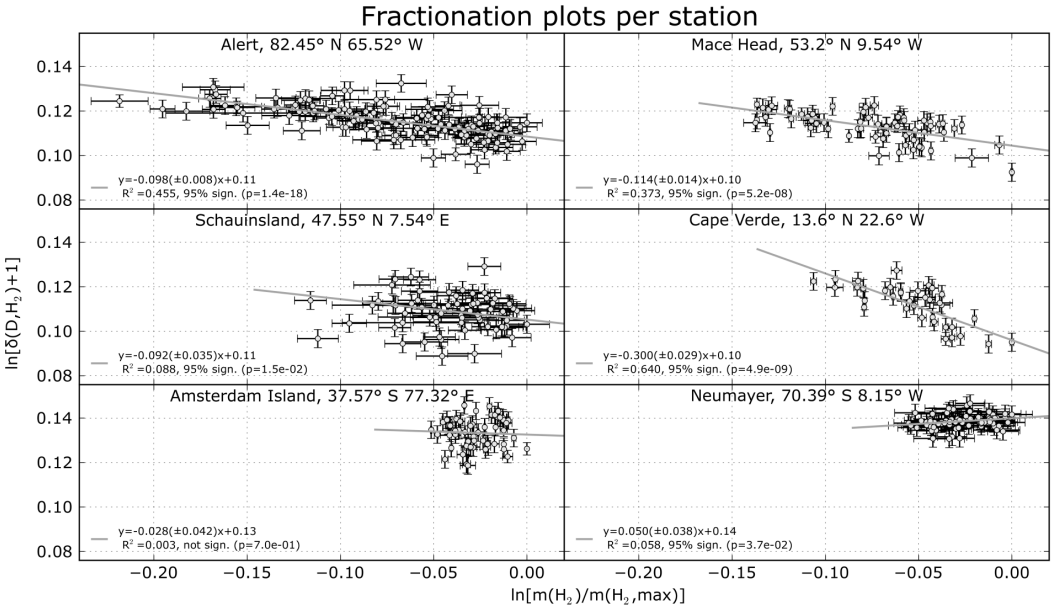

Fig. 5. Fractionation plots of the datasets from the different stations. Plotted are $\ln(\delta(\mathrm{D})+1)$ vs. $\ln(m(\mathrm{H_2})/m(\mathrm{H_2},\mathrm{max}))$ with $m(\mathrm{H_2})$ the mixing ratio and $m(\mathrm{H_2},max)$ the maximum mixing ratio found. Grey lines are the fitted lines obtained from the Weighted Total Least-Squares fitting routine. Error bars indicate one standard deviation. Indicated errors in the fit parameters indicate one standard error. R^2 is the squared correlation coefficient and p is the p-value for the F statistic, both calculated as for an "ordinary" least-squares fitted line.

ACPD
11, 10087–10120, 2011

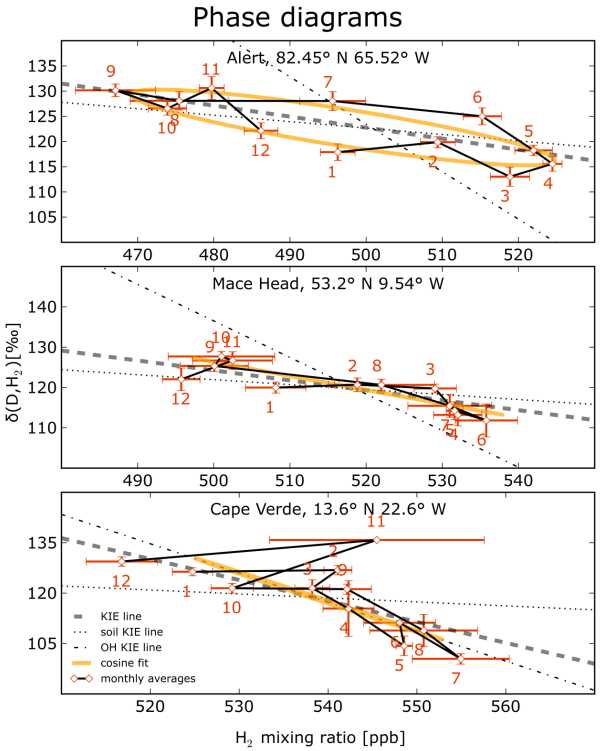

Fig. 6. Phase diagrams (δ(D) vs. $m(H_2)$) of the monthly averages (labelled with month number) of the three stations that show clear seasonal cycles. The orange ellipses are derived from the sinusoidal fits to the time series. The thick grey dashed line is the "KIE" line for the apparent fractionation factor determined from the fractionation plot for the respective station as defined in (Allan et al., 2001). The dotted and dash-dotted lines are the KIE lines for the two different sink processes, with values for α from (Rhee et al., 2006b). Note that the determined KIE line at Alert and Mace Head is closest to the soil uptake KIE line, while the determined KIE line at Cape Verde is closer to the OH oxidation KIE line.

ACPD
11, 10087–10120, 2011

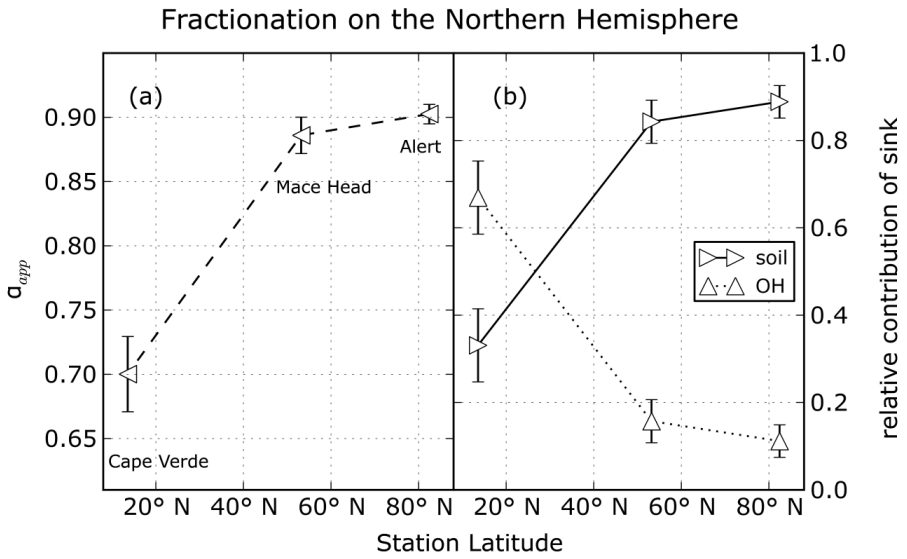

Fig. 7. (a) Apparent fractionation factors for the NH, calculated from a least-squares fit to a Rayleigh plot, plotted as a function of station latitude. **(b)** Relative contributions of uptake by soils and atmospheric oxidation by OH to the total sinks, calculated from the apparent fractionation factors and the values for the fractionation processes used by Rhee et al. (2006b). Error bars indicate one standard error.

ACPD
11, 10087–10120, 2011